



Contents lists available at ScienceDirect

## Biochemical Pharmacology

journal homepage: [www.elsevier.com/locate/biochempharm](http://www.elsevier.com/locate/biochempharm)1  
2 **Analogs of MK-499 are differentially affected by a mutation in the S6 domain**  
3 **of the hERG K<sup>+</sup> channel**4 Jerzy Karczewski<sup>a,1,\*</sup>, Jixin Wang<sup>a,1</sup>, Stefanie A. Kane<sup>a</sup>, Laszlo Kiss<sup>a</sup>, Kenneth S. Koblan<sup>a</sup>,  
5  $\alpha_1$ J. Christopher Culberson<sup>b</sup>, Robert H. Spencer<sup>a,2</sup>6 <sup>a</sup> Department of Pain Research, Merck Research Laboratories, West Point, PA, United States7 <sup>b</sup> Department of Medicinal Chemistry, Merck Research Laboratories, West Point, PA, United States

## ARTICLE INFO

## Article history:

Received 28 December 2008

Accepted 17 February 2009

Available online xxx

## Keywords:

hERG potassium channel

MK-499

Ion channel pharmacology

Site-directed mutagenesis

Molecular modeling

## ABSTRACT

Drug-induced long QT syndrome has been principally ascribed to block of the cardiac hERG K<sup>+</sup> channel. Methanesulfonanilides, such as MK-499, E-4031 and dofetilide, are potent hERG antagonists that likely bind along the S6 helix within the inner vestibule of the pore. To further investigate these interactions, we broadly explored the structure–activity relationships of closely related analogs of MK-499 using a high-throughput ion flux assay, and evaluated in greater detail using patch-clamp electrophysiology. We observed that substitutions at the 4-position on the benzopyran ring significantly affected the potency of these analogs with the rank order of unsubstituted  $\approx$  ketone > amine > hydroxyl, implicating an important interaction at this position. We also evaluated the potency of these analogs on an S6 mutant of hERG (F656A) previously shown to significantly reduce the affinity for MK-499 and other known hERG antagonists (e.g. cisapride, terfenadine). In contrast to MK-499 (4-hydroxyl) and either the amine or unsubstituted analogs, the potency of the ketone analog was unaffected by this mutation suggesting that a compensatory interaction may be unveiled with the aromatic to apolar substitution, possibly through hydrogen bonding with Ser624 based on molecular modeling. More significantly, we found that this mutation rendered hERG susceptible to block in the closed-state by the smaller, unsubstituted analog, but not by MK-499 or larger analogs. Together these data suggest that interaction with Phe656 is not an absolute requirement for the binding of all methanesulfonanilide compounds, and that this residue may play a broader role in regulating access to the inner vestibule.

© 2009 Published by Elsevier Inc.

8  
9  
10 **1. Introduction**

11 Since the identification of the *HERG*<sup>1</sup> gene (KCNH2), which  
12 encodes a rapidly inactivating delayed-rectifier K<sup>+</sup> channel  $\alpha$   
13 subunit, as the molecular entity underlying the *I<sub>Kr</sub>* current in  
14 human heart [1,2], a vast amount of information has implicated  
15 this channel in both congenital and acquired forms of long QT  
16 syndrome (LQTS)—a disorder associated with an increased risk for  
17 ventricular tachyarrhythmia (torsade de pointes) that can degener-  
18 erate into ventricular fibrillation and sudden death [3]. Although

hERG is expressed in a variety of tissues [4], its critical functional  
role in the repolarization phase of the cardiac action potential, in  
addition to *I<sub>Ks</sub>* (KvLQT1), has provided the impetus for a detailed  
understanding of the structure and function of this channel. Inherited  
mutations which alter either the function or level of expression of  
hERG (KCNH2) have been linked to a form of LQTS known as LQT2  
[3,5]. Acquired, or drug-induced, LQTS has been primarily, if not  
exclusively, associated with compounds which can block hERG. These  
include several Class III antiarrhythmics (e.g. dofetilide, sotalol) as  
well as a plethora of structurally distinct drugs encompassing  
antihistamines, antimicrobials, GI prokinetic and psychotropic  
agents (reviewed in [6]).

Significant advances have been made in the identification of  
residues within the pore of hERG responsible for the binding of  
these drugs with the intention of developing a pharmacophore  
model that could be applied for reducing or eliminating the  
potential for drug-induced QT prolongation [7,8]. In this study, we  
have utilized a high-throughput Rb<sup>+</sup> efflux assay together with  
whole-cell patch-clamp analysis to develop a refined model for

\* Corresponding author at: Merck Research Laboratories, WP26A-2000, P.O. Box 4, West Point, PA 19486, United States. Tel.: +1 215 652 3505; fax: +1 215 652 0800.

E-mail address: [jerzy\\_karczewski@merck.com](mailto:jerzy_karczewski@merck.com) (J. Karczewski).

<sup>1</sup> Both authors contributed equally to this work.

<sup>2</sup> Current address: Cara Therapeutics, Inc., Shelton, CT 06484, USA.

Abbreviations: AAS, atomic absorption spectrometry; *HERG*, human ether-a-go-go related gene (KCNH2); hERG, ether-a-go-go-related potassium channel protein; Kv, voltage-gated K<sup>+</sup> channel; LQTS, long QT syndrome; CHO, Chinese hamster ovary.

drug interactions within hERG. Rather than broadly investigating the activities for a variety of structurally unrelated chemotypes on a series of hERG mutants, we chose to study a series of close analogs of the well-characterized hERG antagonist MK-499 on the wild-type channel, and on a single site mutation (F656A) previously reported to dramatically affect the potency of this and several other hERG blockers. This choice allowed us to probe the details of molecular interactions between this inhibitor and the hERG channel in a limited structural series. It is anticipated that the observed interactions will provide insights that are pertinent not only to methanesulfonanilide antagonists but also to compounds from other structural classes.

## 2. Materials and methods

### 2.1. Materials

MK-499, all structurally related analogs, and sertindole, were synthesized in the Department of Medicinal Chemistry at Merck Research Laboratories. Cisapride, astemizole and all other chemicals were obtained from Sigma Aldrich Corp. (St. Louis, MO, USA).

### 2.2. Molecular biology

The hERG/pSP64 construct was provided by Sanguinetti et al. [2]. hERG was cloned into pCDNA5/FRT vector between HindIII and BamHI and used to generate a stable CHO cell line. To generate the F656A point mutation in hERG, site-directed mutagenesis was performed using methylated hERG/pSP64 according to the GeneTailor method (Invitrogen, Carlsbad, CA, USA). After amplification, mutated unmethylated product was selected in DH5 $\alpha$  *E. coli* cells. The 176 bp cassette between BglII and XhoI containing the target site was swapped into WT hERG/pCDNA5/FRT. WT and F656A hERG constructs were confirmed by restriction mapping and DNA sequencing.

### 2.3. Expression of hERG and F656A mutant in Flp-In CHO cells

hERG and the F656A mutant were expressed in CHO cells using the Flp-In system (Invitrogen). Flp-In host CHO cells containing a single integrated Flp Recombination Target (FRT) site were cotransfected using Lipofectamine 2000 (Invitrogen). For each transfection, 0.4  $\mu$ g hERG/pCDNA5/FRT (or F656A hERG/pCDNA5/FRT) and 3.6  $\mu$ g pOG44 (for expression of the Flp recombinase) were incubated with Flp-In CHO cells for 5 h in Opti-MEM I serum-free medium (Invitrogen). The stable expression cell line was selected by culturing cells in the presence of 200  $\mu$ g/ml hygromycin. The cells were maintained in F-12 medium containing 10% FBS, 100 U/ml penicillin, 100  $\mu$ g/ml streptomycin, 200  $\mu$ g/ml hygromycin at 37 °C with 5% CO<sub>2</sub>. The expression of hERG or F656A hERG was confirmed by Western Blot analysis using anti-hERG antibody (Alomone Labs. Ltd., Jerusalem, Israel).

### 2.4. Rubidium efflux assay

CHO cells were seeded in 96-well V-bottom microtiter plates at  $4 \times 10^4$  cells per well and allowed to grow for 48 h. The medium was then aspirated, Rb-Load Buffer (Aurora Biomed, Vancouver, Canada) containing 5.4 mM RbCl was added, and cells were incubated at 37 °C for 3 h to obtain maximal loading [9]. The Rb-Load Buffer was washed off the cells with  $5 \times 200 \mu$ l/well of Hanks' Balanced Salt Solution (HBSS). Drugs were dissolved in 92 DMSO at 10 mM concentration, serially diluted into 100  $\mu$ l HBSS, and added to cells for 10 min. The cells were subsequently depolarized by the addition of 100  $\mu$ l/well of  $2 \times$  depolarization

buffer (HBSS modified by the replacement of 100 mM NaCl with 100 mM KCl). After 10 min incubation at room temperature, the supernatant was transferred into a clean 96-well plate and cell lysis buffer (200  $\mu$ l/well) was added to the assay plate to release intracellular Rb<sup>+</sup> (Aurora Biomed, Vancouver, Canada). All liquid handling was performed using a Biomek FX Laboratory Workstation (Beckman Coulter Inc., Fullerton, CA, USA).

The Rb<sup>+</sup> concentration was measured in both the supernatant and the cell lysate (100  $\mu$ l sample of each) using an automated atomic absorption spectrophotometer (Model: ICR-8000; Aurora Biomed, Vancouver, Canada). Rb<sup>+</sup> efflux was calculated using Equation I: %efflux =  $100 \times (\text{Rb}_{\text{sup}}^+ / (\text{Rb}_{\text{sup}}^+ + \text{Rb}_{\text{lys}}^+))$ . In order to quantify the effect of drugs, the data was converted into %inhibition calculated using Equation II: %inhibition =  $100 - ((\text{efflux}_{\text{drug}} - \text{efflux}_{\text{min}}) / (\text{efflux}_{\text{max}} - \text{efflux}_{\text{min}}))$ , where efflux<sub>drug</sub> is the Rb<sup>+</sup> efflux in the presence of tested drug, efflux<sub>min</sub> is the Rb<sup>+</sup> efflux in the presence of 10  $\mu$ M astemizole, efflux<sub>max</sub> is the Rb<sup>+</sup> efflux in the presence of 0.25% DMSO. Nonlinear regression analysis was used to calculate the IC<sub>50</sub> values using the program Prism (GraphPad Software, San Diego, CA).

Due to the low level of functional expression (i.e. low signal-to-noise) we initially observed for the F656A mutant in CHO cells and also reported for its expression in *Xenopus* oocytes [8], cells were preincubated at 30 °C for 48 h which increased the current density by ~55%, as verified by patch-clamp analysis (data not shown). The use of low temperature or chemical chaperones to facilitate surface expression of hERG mutants, as well as other membrane proteins, has been reported [10–12].

### 2.5. Voltage-clamp recordings

Cells for electrophysiological study were transferred to an 80  $\mu$ l RC-24 recording chamber (Warner Instrument Corp., Hamden, CT, USA) and superfused with a Hank's Balanced Salt Solution (Invitrogen) containing (mM): 137.97 NaCl, 1.26 CaCl<sub>2</sub>, 0.49 MgCl<sub>2</sub>, 0.41 MgSO<sub>4</sub>, 5.33 KCl, 0.44 KH<sub>2</sub>PO<sub>4</sub>, 4.17 NaHCO<sub>3</sub>, 0.34 Na<sub>2</sub>HPO<sub>4</sub>, 5.56 D-glucose, pH 7.3, at a flow rate of 0.8 ml/min, allowing rapid solution changes. K<sup>+</sup> currents were recorded using the whole-cell patch-clamp technique at room temperature (23  $\pm$  1 °C). An Axopatch 200A patch-clamp amplifier was connected through a Digidata 1200 interface (Molecular Devices, Sunnyvale, CA, USA). Patch pipettes were fabricated from capillary glass tubing obtained from Warner Instrument Corp. (1.16–1.5  $\times$  750 mm; #G85150T-3) using a vertical micropipette puller (L/M-3p-A, LIST-MEDICAL, Darmstadt, Germany). Pipette resistances were 2–4 M $\Omega$  when filled with a solution containing (mM): 119 K<sup>+</sup>-gluconate, 15 KCl, 3.2 MgCl<sub>2</sub>, 5 EGTA, 5 K<sub>2</sub>ATP, 5 HEPES, pH 7.35. Cell capacitance and series resistance were compensated (80–90%) before recording. Data were acquired and analyzed using pCLAMP9 (Molecular Devices) and results were plotted using SigmaPlot (Systat Software, Chicago, IL, USA).

### 2.6. Molecular modeling

The 1BL8 KcsA structure was retrieved from the Protein Data Bank. The KcsA structure was used as the template structure for a homology model created by using the MODELER module within INSIGHTII (Ver. 98.0; Accelrys, San Diego, CA, USA). The sequence alignment from Doyle et al. [13] was used to generate the homology model. Subsequent molecular modeling was done with the Merck molecular modeling system (MIX). One hundred low-energy conformations of MK-499 were generated and docked by using the FLOG (Flexible Ligands Oriented on Grid) procedure [14]. Subsequently the docked conformations were energy minimized with macromodel using the MMFF force field [15] while allowing the side chains within 10 Å of the ligand to flex while holding the backbone rigid [16].

### 3. Results

#### 3.1. Initial characterization of hERG antagonists using atomic absorption spectrometry

Due to the unique functional properties of ion channels, the rapid evaluation of compounds that modulate their function has posed a difficult challenge. In order to investigate the structure–activity relationships for a broad series of chemical entities against hERG, we utilized a non-radioactive ion flux assay using atomic absorption spectrometry (AAS) which has shown utility for rapidly evaluating the pharmacological properties of several voltage- and ligand-gated ion channels [17].

The application of AAS for determining the pharmacology of the hERG K<sup>+</sup> channel has been reported and involves loading the cells with nonradioactive Rb<sup>+</sup> and measuring the potency of antagonists by the inhibition of Rb<sup>+</sup> efflux upon membrane depolarization with high extracellular K<sup>+</sup> [18]. To optimize the conditions for this assay, CHO cells expressing hERG were loaded with RbCl, washed with Hank's buffer to remove the extracellular Rb<sup>+</sup>, and then depolarized by the addition of increasing concentrations of KCl (equimolar substitution for NaCl) (Fig. 1A). Rb<sup>+</sup> efflux was then measured in the supernatant and cell lysate using an automated atomic absorption spectrophotometer (see Section 2). Maximal efflux of Rb<sup>+</sup> from CHO-hERG cells was attained with 50 mM KCl, and no further increase was observed with concentrations up to 140 mM (EC<sub>50</sub> = 22 mM KCl). To ensure that the kinetic endpoint for efflux was being attained, the Rb<sup>+</sup> concentration was measured in the supernatant from cells depolarized for varying lengths of time, and maximal

efflux was observed after 10 min (data not shown). The addition of 10 μM astemizole, a potent inhibitor of hERG, completely blocked the efflux of Rb<sup>+</sup> demonstrating that ion permeation was specific to the heterologously expressed hERG channel. Minimal Rb<sup>+</sup> efflux was observed in untransfected CHO cells, consistent with the lack of native outward K<sup>+</sup> conductance in these cells [19,20].

To evaluate the pharmacology of hERG in this assay, the dose–response relationship for several known antagonists was determined using these methods (Fig. 1B). The IC<sub>50</sub> values for these compounds as measured with this assay are somewhat higher than values reported using single-cell patch-clamp analysis, but they are consistent with the known pharmacology of hERG and with values reported using other functional, high-throughput techniques [18,21,22]. Although some of these compounds display positive voltage-dependent block which cannot be readily investigated by AAS due to technical limitations (i.e. the membrane cannot depolarize to positive potentials) [23–25], general structure–activity relationships were readily identified and informative for more definitive analysis by patch-clamp electrophysiology.

#### 3.2. Substituents on pyran ring influence potency of MK-499 analogs on hERG

To characterize the structure–activity relationships for a series of MK-499 analogs, we determined their relative potency

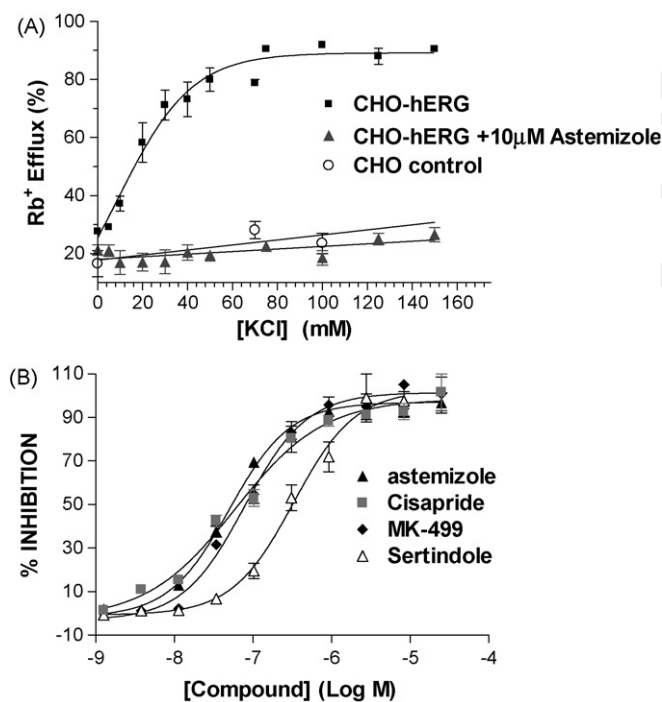


**Fig. 1.** Analysis of Rb<sup>+</sup> efflux for the hERG channel expressed in CHO cells and dose-dependent inhibition using known blockers. (A) Increasing concentrations of KCl were used to depolarize the cell membrane and initiate Rb<sup>+</sup> efflux from cells expressing the hERG channel. The Rb<sup>+</sup> concentration in the supernatant and lysate was measured by automated atomic absorption spectrometry (AAS) and the percent efflux calculated as described in Section 2. Untransfected CHO K1 cells were used as a negative control. Astemizole (10 μM) was used as a positive control to determine full block in CHO-hERG cells. (B) A series of known hERG antagonists were preincubated with CHO-hERG cells at increasing concentrations for 10 min. prior to activation with 50 mM KCl. Rb<sup>+</sup> efflux was determined using AAS and the percent inhibition was calculated as described in Section 2. The observed IC<sub>50</sub> values were 53 (±4.8) nM, 67 (±4.9) nM, 107 (±5.7) nM, and 355 (±16.7) nM for astemizole, cisapride, MK-499 and sertindole, respectively (*n* = 3–6).

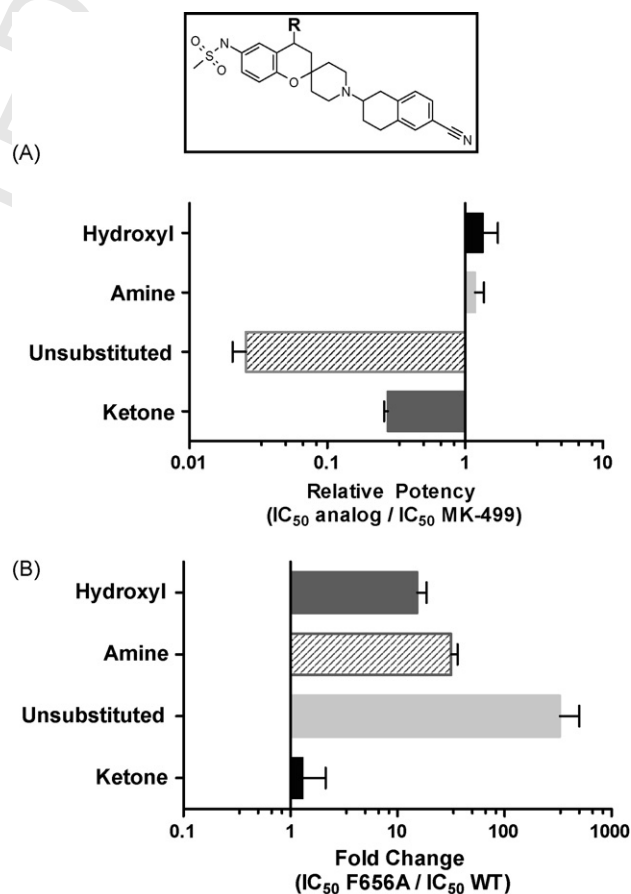


**Fig. 2.** Effect of R-group substitutions on the potency of analogs of MK-499 on WT hERG and the F656A mutant using the AAS Rb<sup>+</sup> efflux assay. (A) The potency of stereoisomers of MK-499 (hydroxyl) as well as amine, ketone and unsubstituted analogs on the R-4 position of the pyran ring (see inset) were determined on WT hERG. The relative potency of these structural analogs compared to that for MK-499 is plotted on a log scale (mean ± SEM). (B) The potency of the same structural analogs of MK-499 was evaluated on the F656A mutant hERG channel. The relative effect of this mutation on the potency of these analogs is shown relative to their activity on WT hERG (mean ± SEM).

207 against the wild-type hERG channel using AAS. From these  
 208 results, we observed significant effects on compound potency  
 209 due to substitutions at the 4-position on the pyran ring (Fig. 2A).  
 210 In comparison to MK-499 which has a hydroxyl at this position,  
 211 unsubstituted or ketone-substituted analogs were 4–35-fold  
 212 more potent (average  $IC_{50}$  values, 3 and 26 nM, respectively)  
 213 against hERG. This result is consistent with a previous study that  
 214 found a ketone analog of MK-499 (L-702,958) had greater  
 215 potency for block of the native  $I_{Kr}$  current in guinea pig  
 216 ventricular myocytes [ $IC_{50}$  values for MK-499 and L-702,958,  
 217 43.9 and 14.6 nM, respectively] [26]. In contrast to the increased  
 218 potency observed with the ketone or unsubstituted analogs,  
 219 amine substitutions at this position were essentially equipotent  
 220 to MK-499 and other hydroxyl analogs.

### 221 3.3. Differential sensitivity of MK-499 analogs to the F656A mutation 222 in hERG

223 To further explore the binding site for MK-499, we evaluated  
 224 these same analogs with a single-site alanine mutation at position  
 225 F656 in the S6 domain of hERG. This mutation has been shown to

226 have the greatest effect on the potency of MK-499 in *Xenopus*  
 227 oocyte voltage-clamp studies, suggesting a critical requirement for  
 228 contacts between MK-499 and this aromatic side chain [8].  
 229 Additionally, the potencies of dofetilide, a related methanesulfo-  
 230 fanilide, and quinidine were reduced by 120-fold and 25-fold,  
 231 respectively, when F656 was mutated to valine [27], suggesting  
 232 that small hydrophobic groups are not sufficient replacements for  
 233 this residue.

234 Consistent with these data, we observed a significant  
 235 reduction in the potency for MK-499 and related stereoisomers  
 236 against the hERG F656A mutant in the AAS assay (Fig. 2B). The  
 237 potency of amine and unsubstituted analogs of MK-499 were  
 238 also significantly less potent on the F656A mutant channel with  
 239 a >10-fold decrease in the  $IC_{50}$  compared to wild-type hERG.  
 240 However, quite surprisingly, we observed that ketone analogs of  
 241 MK-499, such as L-702,958, were nearly equipotent on the wild-  
 242 type and F656A mutant channels. This suggested that F656 may  
 243 not be obligatory for the binding of all methanesulfonanilide  
 244 compounds. These findings were then used to guide studies  
 245 using classical patch-clamp analysis to further investigate these  
 246 interactions.

**Table 1**  
 Q2  $IC_{50}$  values for block of WT and F656A hERG channels by MK-499 and structural analogs.

	R-group	$IC_{50}$ (Nm)		Relative potency ( $IC_{50}$ F656A/ $IC_{50}$ WT)
		WT	F656A	
MK-499 (R,R)	Hydroxyl	89.8 ± 9.7	2057 ± 271	22.9
Compound 2 (S,S)	Hydroxyl	107 ± 19.6	1705 ± 174	15.9
Compound 3	Amine	29.2 ± 7.0	356 ± 43	11.5
Compound 4	Unsubstituted	5.0 ± 0.7	211 ± 27	42.2
L-702,958	Ketone	14.3 ± 1.1	29.2 ± 2.9	2.0

Steady-state block was determined from tail currents elicited by depolarization from the holding potential of -90 to 0 mV for 5 s, followed by hyperpolarization to -140 mV for 256 ms. The  $IC_{50}$  values indicated represent the average  $IC_{50} \pm SEM$  from individual cells at each dose ( $n = 2-6$ ).

### 3.4. Electrophysiological evaluation of the potency of MK-499 analogs on WT and F656A hERG channels currents

Based upon the initial structure–activity relationships identified using AAS, we evaluated the potency of MK-499, its enantiomer (Compound 2), and three analogs containing either an amine, dihydrogen (unsubstituted), or ketone at the 4-pyran position. Consistent with the results from AAS, the unsubstituted and ketone analogs of MK-499 were more potent than MK-499, its enantiomer, or the amine analog (Compound 3) on the WT hERG channel (see Table 1).

We then examined the effect of the F656A mutation on the potency of these same compounds. Although readily measurable, currents for the F656A mutant channel stably expressed in CHO cells were significantly lower compared to the WT channel (see Fig. 3), as has been previously reported [8,28]. Consistent with results from the AAS assay, MK-499, its enantiomer, and the amine and unsubstituted analogs showed a significant right-shift in their  $IC_{50}$  values compared to the WT hERG channel (Table 1),

confirming previous reports that binding interactions with F656 are critical for hERG block. However, currents for the F656A mutant were blocked with nearly equal potency by the ketone analog (L-702,958), similar to our results using the AAS assay (Fig. 3). This suggested that the keto oxygen of L-702,958 may be participating in a unique binding interaction within the hERG pore that distinguishes it from MK-499 and other analogs.

### 3.5. Docking model identifies potential hydrogen bonding interactions with S624

In order to understand these results from a structural perspective, we explored docking studies of MK-499, the hydroxyl enantiomer (Compound 2), and the other analogs (Compound 3, Compound 4, and L-702,958) into the homology model of the hERG channel previously described by Mitcheson et al. [8]. Initial dockings of MK-499 analogs were done with a homology model based on the KcsA crystal structure. A second round of docking experiments were done using a model based on an MthK template

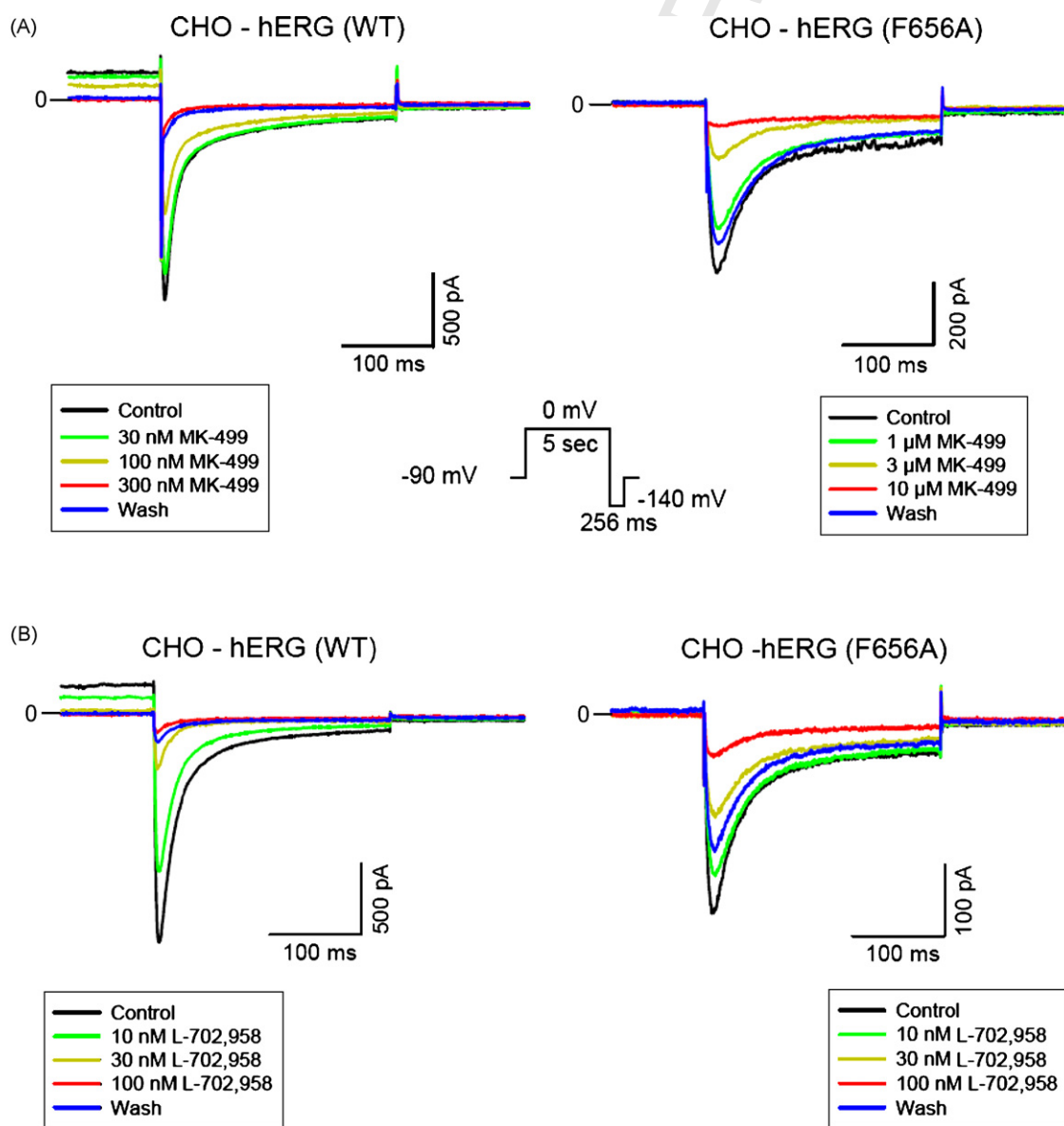


**Fig. 3.** The potency of structural analogs of MK-499 on hERG currents is differentially affected by the F656A mutation. Whole-cell recording of tail currents from WT and F656A hERG channels elicited by depolarization from the holding potential of  $-90$  to  $0$  mV for  $5$  s, followed by hyperpolarization to  $-140$  mV for  $256$  ms. (A) Steady-state block by MK-499 was evaluated on the WT and F656A hERG channels. (B) Steady-state block by the ketone analog (L-702,958) on WT and F656A hERG channels. Recovery from block is also shown for the same cells by measuring the tail currents after  $30$  pulses following washout of the maximal drug concentration tested.

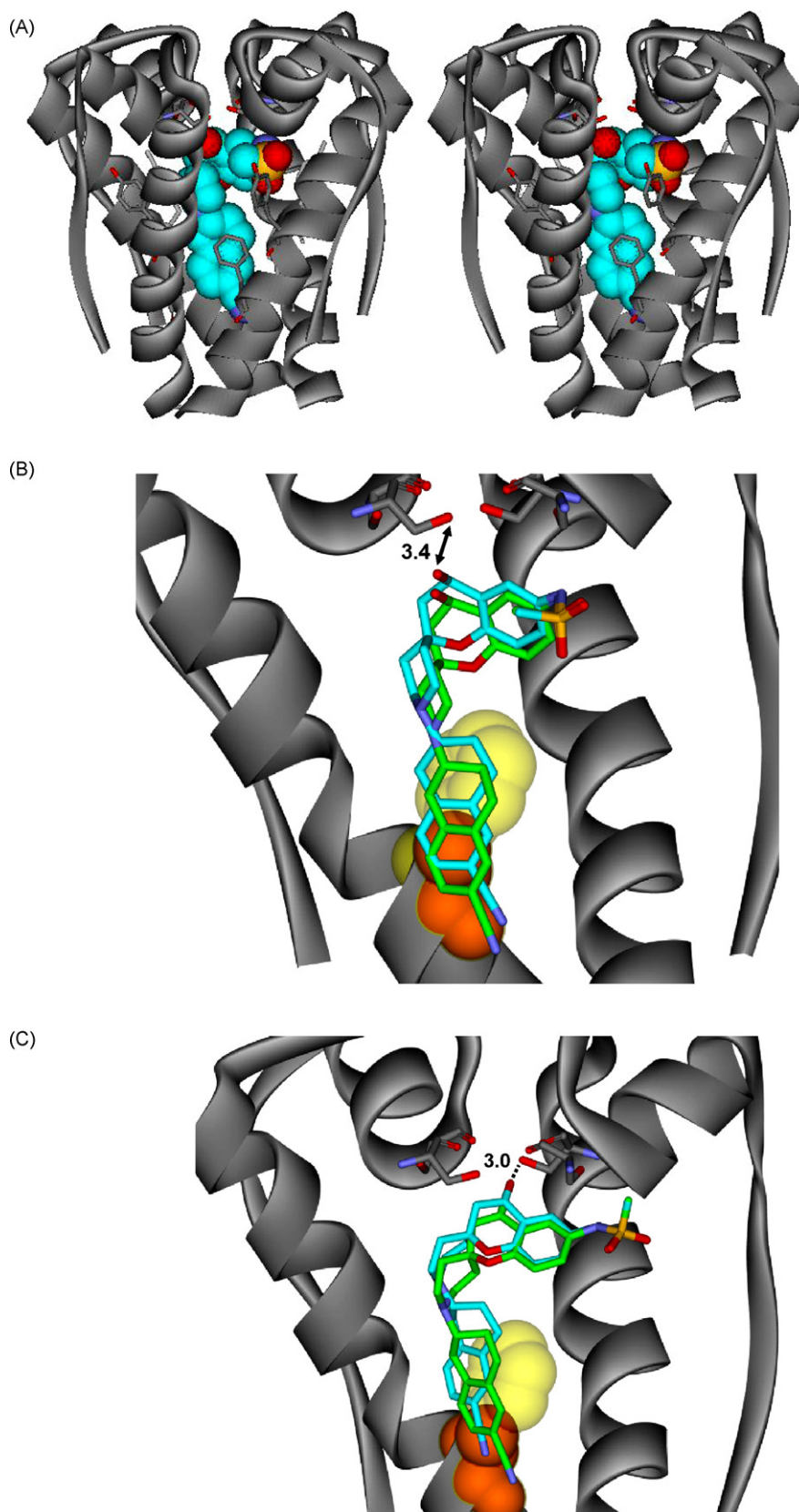


**Fig. 4.** Docking of MK-499 and ketone analog in the pore of hERG using a homology model. (A) Stereoview of the S5-S6 domain of the hERG channel with MK-499 (space-filling model) docked within the pore region. Sidechains for S624, Y652 and F656 are also shown. (B) Close-up view of the energy minimized structure of MK-499 docked within the pore of the wild-type (cyan) and the F656A mutant (green) channels. Sidechain atoms for residue 656 in the wild-type (yellow) and the F656A mutant (red) are also shown as CPK models. The closest approach heavy atom-to-heavy atom distance (3.4 Å) between S624 and MK-499 is indicated. (C) Docked and energy minimized structures of the ketone analog, L-702,958, in the wild-type (cyan) and the F656A (green) mutant channel. The heavy atom-to-heavy atom distance (3.0 Å) between S624 and L-702,958 is indicated.

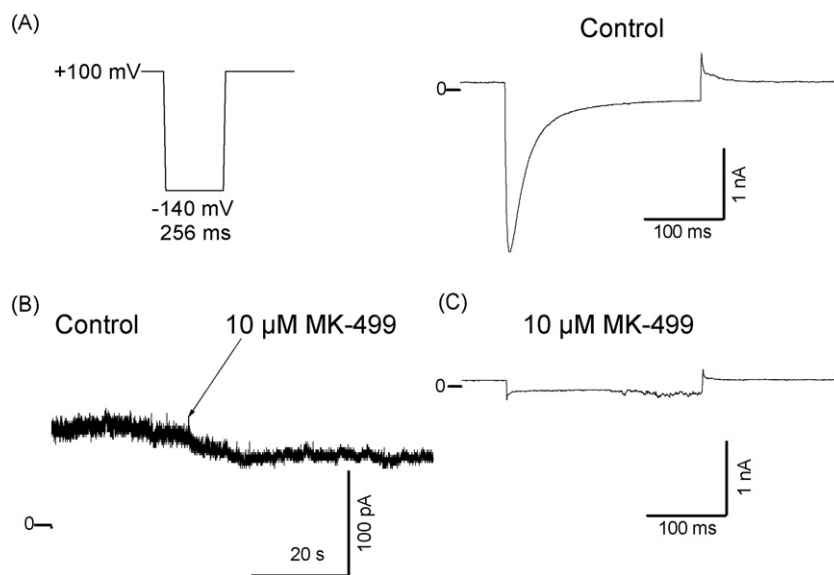


**Fig. 5.** Block of the WT hERG channel in the inactivated state by MK-499. The WT hERG channel was forced into the inactivated state by holding the membrane potential at +100 mV for 20 s, followed by a rapid hyperpolarization step to -140 mV for 256 ms to elicit an inward tail current. (A) Tail current from WT hERG after holding the channel in the inactivated state (at +100 mV) in the absence of drug. (B) Addition of 10 μM MK-499 to the holding current of WT hERG channel while held in the inactivated state at +100 mV for 1 min (leak conductance was not subtracted). (C) Tail current elicited during the first pulse from the WT hERG channel in the presence of 10 μM MK-499 added while holding the channel in the inactivated state (+100 mV).

(model of the open channel state), but the conclusions from either model are similar. From this study, we identified a key hydrogen bonding (H-bond) interaction between S624 and the hydroxyl group of MK-499, and its enantiomer. Although a modest energetic contribution was initially observed for S624 and the binding of MK-499 [8], it is too long range (3.4 Å, hydroxyl oxygen to S624 sidechain) to be considered a classical H-bond, and thus likely contributes minimally to its total binding energy (Fig. 4A and B).

To further extend these observations, we also performed a docking analysis with the F656A mutant channel. These results suggested that replacement of F656 with alanine would cause MK-499 and Compound 2 to move deeper into the pore to gain interactions along S6, thereby losing any weak contact with S624. However, the ketone analog (L-702,958) retained the hydrogen bond to S624 in both the native and mutant channels (Fig. 4C). This model thus provides a structural hypothesis consistent with the functional results obtained with the MK-499 analogs for both the native and mutant hERG channels.

### 3.6. Block of hERG by MK-499 in the open-inactivated state

The relative position of F656 along the S6 helix of hERG (likely near the apex of the inverted teepee) suggests that this residue may not only play a role in drug binding, but also in drug access to the inner pore of the channel. Previous studies have shown that methanesulfonanilides such as MK-499 and dofetilide block hERG in the open state, and that drug-trapping during inactivation likely explains the slow recovery from block [29]. The interaction of propafenone with F656 is also regulated by the transition from the closed to open state [30]. This may be due to conformational changes required for accessibility of drug to the pore and/or to residues involved in high-affinity drug interactions. It has also been shown that hERG remains susceptible to block by MK-499 following removal of C-type inactivation, suggesting that the pore may become accessible to drug upon membrane depolarization due to conformational changes associated with movement of the S4 voltage-sensor with concomitant rearrangements of the S6 helices.

To further explore this question, we investigated whether MK-499 could block the WT hERG channel in the fully inactivated state. By holding the membrane at a strongly depolarized potential the flow of K<sup>+</sup> ions would be blocked due to C-type inactivation, but the voltage-sensor would remain in the activated state. To force hERG into the inactivated state, the membrane was held at +100 mV for 20 s prior to the addition of MK-499 for an additional 60 s (Fig. 5). In the absence of drug, a large inward current was elicited following a rapid hyperpolarizing step to -140 mV. However, nearly complete block was observed with the addition of 10 μM MK-499, suggesting that the drug could access the inner pore following conformational changes associated with activation gating.

### 3.7. Closed channel block of F656A mutant by an MK-499 analog

Although hERG is blocked in the open and inactivated states from the intracellular side of the channel, it does not appear to be blocked in the closed state by methanesulfonanilide compounds like MK-499, dofetilide and E-4031 [31,32]. Accessibility of the pore to these drugs is likely restricted by a physical barrier near the intracellular side of S6. To address whether F656 may play some role in regulating access to the pore, we compared the ability of MK-499 and the smaller, unsubstituted analog (Compound 4) to block the WT and F656A hERG channel in the closed state. Similar to previous studies, there was little or no accumulation of closed-channel block by MK-499 in either the WT or F656A mutant channels (Fig. 6A and B). There was also no closed-channel block of the WT hERG observed using Compound 4 (Fig. 6B). However, in contrast to MK-499, significant closed-channel block of the F656A mutant channel (>50% at 1 μM) was seen with Compound 4 (Fig. 6A). The ketone analog, L-702,958, was also unable to block the closed state of F656A hERG (data not shown). This result clearly indicates that Compound 4 can gain access to pore with the substitution of the bulky phenylalanine residue for alanine at position 656.

Since Compound 4 is ~0.8 Å narrower than MK-499 or L-702,958 (all are of equal length), this suggests that F656 likely acts as a physical barrier to restrict access to the pore in the closed state (Fig. 6C). It also suggests that F656 is located at or near the

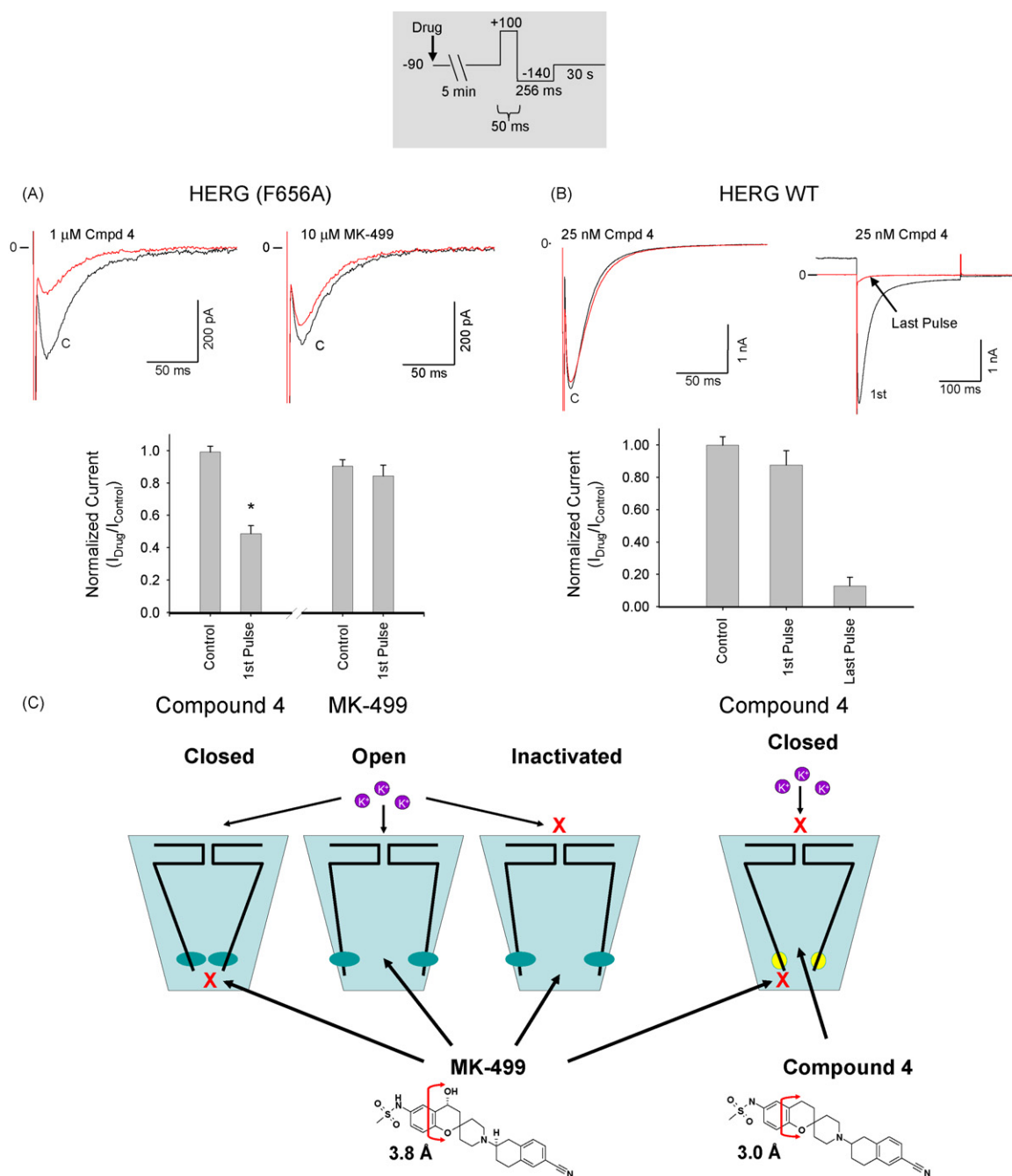


**Fig. 6.** Closed-channel block of the F656A hERG channel by the small, unsubstituted analog of MK-499. Block of WT and F656A hERG in the closed state was evaluated by holding the channel closed at  $-90$  mV while washing on the drug for 5 min, followed by a brief activation step for 50 ms at  $+100$  mV prior to stepping to  $-140$  mV for 256 ms to quantify the hERG tail current. (A) Evaluation of closed-channel block for the F656A hERG channel by MK-499 and the unsubstituted analog (Compound 4) was performed at 5-fold above the  $IC_{50}$  determined for the open state ( $10 \mu\text{M}$  and  $1 \mu\text{M}$  concentrations, respectively). Fractional current was determined from the tail current elicited after the first pulse. Control =  $I_{Last\ pulse}/I_{1st\ pulse}$ ; 1<sup>st</sup> pulse =  $I_{1st\ pulse+Drug}/I_{Last\ pulse-Drug}$  ( $n = 2-3$ ; mean  $\pm$  SEM;  $^*P < 0.05$ ). (B) Evaluation of closed-channel block for the WT hERG channel by the unsubstituted analog (Compound 4) was performed at 5-fold above the  $IC_{50}$  for the open state ( $25 \text{ nM}$ ). Fractional current was determined as described above ( $n = 2-3$ ). Steady-state block for Compound 4 was confirmed on the same cell from the last pulse following activation for 5 s at 0 mV using the protocol described in Fig. 3 (Last Pulse). (C) Model of drug access to the pore of hERG. MK-499 gains access to the pore of WT hERG in the open and inactivated states, but not the closed state. For the F656A hERG mutant, the smaller unsubstituted analog (Compound 4) can block the channel in the closed state, but not the larger parent compound, MK-499.

356 narrowest region of the hERG channel in the closed state. Based on  
357 the maximal distance across Compound 4 ( $3.0 \text{ \AA}$ ), the backbone  $C\alpha$   
358  $-C\alpha$  distance across this region of the pore is likely in the range of  
359  $6 \text{ \AA}$  in the mutant channel.

#### 360 4. Discussion

361 A variety of studies have identified the S6 residue F656 in hERG  
362 as a critical component of drug binding interactions within the

pore of hERG. Although the F656A mutation has an effect on  
363 accelerating the inactivation of hERG, it has been demonstrated  
364 that the position of this aromatic residue along the S6 helix  
365 correlates with its effect on drug binding, and is not due to the  
366 effects on inactivation properties [33]. Additionally, Fernandez et  
367 al. have shown a good correlation between the approximate 2D van  
368 der Waals hydrophobic surface area of the residue at position 656  
369 in hERG and the potency of MK-499, cisapride and terfenadine [34].  
370 Consistent with these observations, our results suggest that the  
371



effect of the F656A mutation on drug binding is primarily due to steric and/or energetic factors. The F656A mutation had been shown to significantly reduce the affinity of several hERG antagonists potentially due to a key hydrophobic or cation–pi interaction with these molecules, particularly MK-499 [8,27].

Although it was initially expected that the potency of all MK-499 analogs would be similarly affected, such is not the case. Subtle differences amongst these analogs can dramatically affect the fold difference in potency brought about by the F656A mutation. Since the loss of interactions with F656 would likely be compensated for by general hydrophobic interactions between the tetrahydro-naphthalene ring and the S6 helix, we focused our attention on the potential interactions with the hydroxyl group at the 4-pyran position in MK-499. Previous studies recognized the importance of S624 in the binding of MK-499 to the channel and characterized the residue as defining the pocket in which the methanesulfone is bound [8]. The results of our study highlight a likely hydrogen bonding interaction between these inhibitors and the sidechain of Ser624 as well. These data help to further define the structural requirements for binding to the hERG channel and in part explain the pharmacological promiscuity of this channel.

The identification of F656 as a key residue involved in drug trapping within the hERG pore suggests that it may play an additional role in regulating accessibility during channel gating. As the channel is cycled between the open, inactivated and closed states to obtain steady-state block, many compounds, including the methanesulfonamides, become trapped and subsequently become very difficult to wash-off. This might be due to the slow rate of drug unbinding compared to the pulse-cycle rate, and/or to high-affinity interactions between the drug and S6 residues which alter open-channel gating.

Based on sequence alignment and a homology model with KcsA, F656 in hERG would be equivalent to Thr107 in KcsA located just below the conserved glycine “gating hinge” identified in the structure of the MthK channel [35]. This is also one of the narrowest regions of the pore in the structure of KcsA, which is likely representative of the closed state [13]. Results from our studies on drug accessibility in the inactivated and closed states of hERG also suggest that F656 is localized in a narrow region of the channel, and can act as a physical barrier from the intracellular aspect of the pore. This may partially explain some of the features of drug trapping observed in hERG since F656 may also act to impede drug egress from the channel. Finally, accessibility of the pore of F656A hERG to the small, unsubstituted analog in the closed-state, but not to MK-499 or larger analogs, provides additional evidence that this residue likely sets the minimal diameter of the pore in the closed state.

Although determining the crystallographic structure of hERG with an inhibitor bound within the pore could validate the interactions that constitute the drug-binding site for this channel, a broader understanding of the molecular landscape which renders it so susceptible to a variety of small molecules may be best understood using techniques which can characterize the channel in its functional state. By applying high-throughput methods to analyze the structure–function relationships with closely related small molecules, a more detailed molecular map of the drug binding site could be rapidly ascertained and probable atomic interactions identified. This approach is similar to that used for mapping toxin binding sites to the extracellular surface of voltage-dependent K<sup>+</sup> channels, and could complement and extend important insights from electrophysiological studies [36–38].

Utilizing this methodology for the hERG K<sup>+</sup> channel, we have established an initial model to account for the differential sensitivities of related compounds to molecular perturbations within the methanesulfonamide binding site. By expanding our study to investigate the impact of mutations near the selectivity

filter and along the length of the S6 helix, we hope to develop a more comprehensive and detailed map of the drug–channel interaction surface. A pharmacophore model based upon these and other data could provide an improved means for facilitating early drug development by the rapid, *in silico* identification of compounds that may cause QT prolongation due to inhibition of the hERG channel.

## Acknowledgements

We would like to thank Dr. Jason Elliott for synthesis of key compounds used in this study, as well as Drs. Joseph J. Lynch, Maria L. Garcia, Christopher J. Dinsmore and B. Wesley Trotter for their helpful suggestions and comments on the manuscript.

## References

- Trudeau MC, Warmke JW, Ganetzky B, Robertson GA. HERG, a human inward rectifier in the voltage-gated potassium channel family. *Science* 1995;269:92–5.
- Sanguinetti MC, Jiang C, Curran ME, Keating MT. A mechanistic link between an inherited and an acquired cardiac arrhythmia: HERG encodes the IKr potassium channel. *Cell* 1995;81:299–307.
- Curran ME, Splawski I, Timothy KW, Vincent GM, Green ED, Keating MT. A molecular basis for cardiac arrhythmia: HERG mutations cause long QT syndrome. *Cell* 1995;80:795–803.
- Wymore RS, Gintant GA, Wymore RT, Dixon JE, McKinnon D, Cohen IS. Tissue and species distribution of mRNA for the IKr-like K<sup>+</sup> channel, *erg*. *Circ Res* 1997;80:261–8.
- Zhou Z, Gong Q, Epstein ML, January CT. HERG channel dysfunction in human long QT syndrome. Intracellular transport and functional defects. *J Biol Chem* 1998;273:21061–6.
- Pearlstein R, Vaz R, Rampe D. Understanding the structure–activity relationship of the human ether-a-go-go-related gene cardiac K<sup>+</sup> channel. A model for bad behavior. *J Med Chem* 2003;46:2017–22.
- Sanchez-Chapula JA, Navarro-Polanco RA, Culbertson C, Chen J, Sanguinetti MC. Molecular determinants of voltage-dependent human ether-a-go-go related gene (HERG) K<sup>+</sup> channel block. *J Biol Chem* 2002;277:23587–95.
- Mitcheson JS, Chen J, Lin M, Culbertson C, Sanguinetti MC. A structural basis for drug-induced long QT syndrome. *Proc Natl Acad Sci USA* 2000;97:12329–33.
- Scott CW, Wilkins DE, Trivedi S, Crankshaw DJ. A medium-throughput functional assay of KCNQ2 potassium channels using rubidium efflux and atomic absorption spectrometry. *Anal Biochem* 2003;319:251–7.
- Zhou Z, Gong Q, January CT. Correction of defective protein trafficking of a mutant HERG potassium channel in human long QT syndrome. Pharmacological and temperature effects. *J Biol Chem* 1999;274:31123–6.
- Thomas D, Kiehn J, Katus HA, Karle CA. Defective protein trafficking in hERG-associated hereditary long QT syndrome (LQT2): molecular mechanisms and restoration of intracellular protein processing. *Cardiovasc Res* 2003;60:235–41.
- Ficker E, Dennis AT, Wang L, Brown AM. Role of the cytosolic chaperones Hsp70 and Hsp90 in maturation of the cardiac potassium channel HERG. *Circ Res* 2003;92:e87–100.
- Doyle DA, Morais Cabral J, Pfuetzner RA, Kuo A, Gulbis JM, Cohen SL, et al. The structure of the potassium channel: molecular basis of K<sup>+</sup> conduction and selectivity. *Science* 1998;280:69–77.
- Kearsley SK, Underwood DJ, Sheridan RP, Miller MD. Flexibase: a way to enhance the use of molecular docking methods. *J Comput Aided Mol Des* 1994;8:565–82.
- Halgren TA. MMFF VI. MMFF94s option for energy minimization studies. *J Comput Chem* 1999;20:720–9.
- Mohamadi F, Richards NGJ, Guida WC, Liskamp R, Lipton M, Caufield C, et al. MacroModel—an integrated software system for modeling organic and bioorganic molecules using molecular mechanics. *J Comput Chem* 1990;11:440–67.
- Terstappen GC. Functional analysis of native and recombinant ion channels using a high-capacity nonradioactive rubidium efflux assay. *Anal Biochem* 1999;272:149–55.
- Tang W, Kang J, Wu X, Rampe D, Wang L, Shen H, et al. Development and evaluation of high throughput functional assay methods for HERG potassium channel. *J Biomol Screen* 2001;6:325–31.
- Hu W, Toral J, Cervoni P, Ziai MR, Sokol PT. Depolarization-induced 86Rb<sup>+</sup> efflux in CHO cells expressing a recombinant potassium channel. *J Pharmacol Toxicol Methods* 1995;34:1–7.
- Robertson B, Owen DG. Pharmacology of a cloned potassium channel from mouse brain (MK-1) expressed in CHO cells: effects of blockers and an ‘inactivation peptide’. *Br J Pharmacol* 1993;109:725–35.
- Kiss L, Bennett PB, Uebele VN, Koblan KS, Kane SA, Neagle B, et al. High throughput ion-channel pharmacology: planar-array-based voltage clamp. *Assay Drug Dev Technol* 2003;1:127–35.

- [22] Cheng CS, Alderman D, Kwash J, Dessaint J, Patel R, Lescoe MK, et al. A high-throughput HERG potassium channel function assay: an old assay with a new look. *Drug Dev Ind Pharm* 2002;28:177–91.
- [23] Suessbrich H, Waldegger S, Lang F, Busch AE. Blockade of HERG channels expressed in *Xenopus* oocytes by the histamine receptor antagonists terfenadine and astemizole. *FEBS Lett* 1996;385:77–80.
- [24] Potet F, Bouyssou T, Escande D, Baro I. Gastrointestinal prokinetic drugs have different affinity for the human cardiac human ether-a-gogo K(+) channel. *J Pharmacol Exp Ther* 2001;299:1007–12.
- [25] Rampe D, Murawsky MK, Grau J, Lewis EW. The antipsychotic agent sertindole is a high affinity antagonist of the human cardiac potassium channel HERG. *J Pharmacol Exp Ther* 1998;286:788–93.
- [26] Lynch Jr JJ, Wallace AA, Stupienski 3rd RF, Baskin EP, Beare CM, et al. Cardiac electrophysiologic and antiarrhythmic actions of two long-acting spirobenzopyran piperidine class III agents, L-702,958 and L-706,000 [MK-499]. *J Pharmacol Exp Ther* 1994;269:541–54.
- [27] Lees-Miller JP, Duan Y, Teng GQ, Duff HJ. Molecular determinant of high-affinity dofetilide binding to HERG1 expressed in *Xenopus* oocytes: involvement of S6 sites. *Mol Pharmacol* 2000;57:367–74.
- [28] Milnes JT, Crociani O, Arcangeli A, Hancox JC, Witchel HJ. Blockade of HERG potassium currents by fluvoxamine: incomplete attenuation by S6 mutations at F656 or Y652. *Br J Pharmacol* 2003;139:887–98.
- [29] Mitcheson JS, Chen J, Sanguinetti MC. Trapping of a methanesulfonanilide by closure of the HERG potassium channel activation gate. *J Gen Physiol* 2000;115:229–40.
- [30] Witchel HJ, Dempsey CE, Sessions RB, Perry M, Milnes JT, Hancox JC, et al. The low-potency, voltage-dependent HERG blocker propafenone—molecular determinants and drug trapping. *Mol Pharmacol* 2004;66:1201–12.
- [31] Spector PS, Curran ME, Keating MT, Sanguinetti MC. Class III antiarrhythmic drugs block HERG, a human cardiac delayed rectifier K<sup>+</sup> channel. Open-channel block by methanesulfonanilides. *Circ Res* 1996;78:499–503.
- [32] Kiehn J, Lacerda AE, Wible B, Brown AM. Molecular physiology and pharmacology of HERG. Single-channel currents and block by dofetilide. *Circulation* 1996;94:2572–9.
- [33] Chen J, Seeböhm G, Sanguinetti MC. Position of aromatic residues in the S6 domain, not inactivation, dictates cisapride sensitivity of HERG and eag potassium channels. *Proc Natl Acad Sci USA* 2002;99:12461–6.
- [34] Fernandez D, Ghanta A, Kauffman GW, Sanguinetti MC. Physicochemical features of the HERG channel drug binding site. *J Biol Chem* 2004;279:10120–7.
- [35] Jiang Y, Lee A, Chen J, Cadene M, Chait BT, MacKinnon R. The open pore conformation of potassium channels. *Nature* 2002;417:523–6.
- [36] Hidalgo P, MacKinnon R. Revealing the architecture of a K<sup>+</sup> channel pore through mutant cycles with a peptide inhibitor. *Science* 1995;268:307–10.
- [37] Ranganathan R, Lewis JH, MacKinnon R. Spatial localization of the K<sup>+</sup> channel selectivity filter by mutant cycle-based structure analysis. *Neuron* 1996;16:131–9.
- [38] Imredy JP, MacKinnon R. Energetic and structural interactions between delta-dendrotoxin and a voltage-gated potassium channel. *J Mol Biol* 2000;296:1283–94.

540  
541  
542  
543  
544  
545  
546  
547  
548  
549  
550  
551  
552  
553  
554  
555  
556  
557  
558  
559  
560  
561  
562  
563  
564  
565